IEEE Access
Multidisciplinary | Rapid Review | Open Access Journal

Received September 6, 2019, accepted September 15, 2019, date of publication September 26, 2019,
date of current version October 15, 2019.

Digital Object Identifier 10.1109/ACCESS.2019.2944054

Near-Field Focused Subarrays in a Multi-Panel Configuration

HSI-TSENG CHOU[1], (Fellow, IEEE), MARCOS R. PINO[2], PAOLO NEPA[3], (Member, IEEE), AND CHANG-YI LIU[4]

[1]Graduate Institute of Communication Engineering, National Taiwan University, Taipei 10617, Taiwan
[2]Department of Electrical Engineering, University of Oviedo at Gijón, 33203 Gijón, Spain
[3]Department of Information Engineering, University of Pisa, 56122 Pisa, Italy
[4]Department of Communication Engineering, Yuan Ze University, Taoyuan 32003, Taiwan

Corresponding author: Hsi-Tseng Chou (chouht@ntu.edu.tw)

This work was supported in part by the Ministry of Science and Technology, Taiwan, from the Ministerio de Educacion, Cultura y Deporte—Programa de Movilidad Salvador de Madariaga, under Grant PRX17/00635, and in part by the Ministerio de Ciencia, Innovación y Universidades, under Project TEC2017-86619-R (ARTEINE).

ABSTRACT This paper investigates the focusing features of a multi-panel near-field focused (NFF) antenna. Differently from conventional NFF *planar* arrays, the proposed configuration is made of a set of NFF subarrays that are concentrically arranged over a cylindrical boundary. A systematic numerical analysis is performed to show how to control the shape of the -3dB focal spot through the main geometrical and electrical parameters of the proposed antenna layout, such as the number of subarrays, the focal spot location of each subarray and the radius of the cylindrical boundary the subarrays are arranged on. When compared with conventional *planar* NFF arrays, the additional mechanical complexity is partially balanced by a simpler feeding network design and a more symmetric focal spot. Experimental results are shown for a prototype operating at the 2.4 GHz ISM band.

INDEX TERMS Antenna arrays, focused arrays, focal spot shaping, near-field communication, near-field focusing, electromagnetic focusing.

I. INTRODUCTION

Applications exploiting short-range radio links are becoming increasingly popular. Typical examples include RFID (Radio Frequency Identification) systems, non-contact microwave sensing, biomedical applications, ground penetrating radars, wireless power and data transfer, near-field communications (NFCs), dedicated short-range communications (DSRCs). In most short-range radio-link scenarios, focusing the field radiated by the transmitter/interrogator can reduce the interferences from nearby scatterers, provide the required radio coverage at a minimum radiated power, enhance the detection resolution and increase the wireless link reliability. In this context, a wide selection of near-field focused (NFF) microwave antennas have been studied by resorting to different technologies and design criteria (the reader can refer to [1], [2] for an updated survey).

In many indoor applications at microwave frequency band, the NFF antennas cannot be electrically large such as those at mm-wave and optical frequencies, due to the space constraints. It follows that the focusing effect in the radiative near-field region may be quite limited, and the -3dB focal spot usually exhibits an elongated shape [3], with a depth of focus (DoF) along the direction orthogonal to the array aperture that is always larger than the width of focus (WoF), the latter being the size of the focal spot in the focal plane parallel to the array aperture. In [4], Blanco *et al.* studied a NFF annular-slot leaky-wave antenna operating at 10GHz, where the normal field component (the one perpendicular to the antenna surface) has been used to complement the tangential component around the focal spot region, in order to obtain a more symmetric focal spot for the total field amplitude. Additional solutions to shape the focal spot by combining a number of NFF antennas can be found in [5], [6], where two linear NFF leaky-wave arrays have been assembled side-by-side, to get a more symmetric focal spot in the plane containing the two arrays. In the context of synthesis techniques for NFF arrays, in [7] a neural network technique has been applied to maximize the radiated field amplitude at an assigned set of focal points. It is also worth mentioning the approach

The associate editor coordinating the review of this manuscript and approving it for publication was Shah Nawaz Burokur.

introduced in [8], where the phase of the field at assigned focal points can be used as a further degree of freedom to shape the near-field, by solving a finite number of convex programming problems. The above method can be used to simultaneously maximize the field at an assigned extended focal region (or multiple focal points) and enforce an upper bound power constraint outside the regions of interest [9]. The above exploitation of the phase of the field at the focal points has been recently included into a modified multi-target time-reversal approach [10]; although the numerical examples in [10] are relevant to reactive near-field scenarios, the proposed technique can also be applied when the regions of interest are at a larger distance from the array, provided that the assigned focal points are quite close. If the latter condition is not met, a simple superposition of the array coefficients synthesized for each distinct focal point may be enough to get an adequate performance [11]. The shaping of the (scalar) near-field by resorting to convex optimization has also been applied in [12] when the antenna radiates in free-space, and then extended in [13] to account for the presence of lossy stratified media. The effect of the amplitude tapering in a planar NFF array has been numerically studied in [14], when all the elements belonging to the same ring of an 8x8 planar array are fed with a uniform amplitude. A projection method in the plane-wave spectral domain has been implemented in [15] for the 3D shaping of the near-field of an antenna aperture. Recently, Cicchetti *et al.* [16], [17] presented an interesting and flexible near-field synthesis procedure based on the eigenfields of the radiation matrix of the antenna array. Once a surface close to the antenna has been assigned, the active power passing through that surface can me optimized or a specific field pattern can be synthesized. The synthesis surface can be either open or surrounding the antenna, while the field synthesis is based on both the electric and magnetic fields, or the electric field only. In [17], a set of different complex near-field distributions have been considered for a numerical validation of the proposed synthesis procedure: tilted Bessel beams, orbital angular momentum (OAM) Bessel beams and Airy beams.

In this paper, the shaping of the -3dB focal spot in the antenna radiative near-field region is achieved by resorting to a NFF *non-planar* antenna, where a set of P NFF subarrays are properly arranged on a cylindrical surface. Numerical simulations of the NFF *non-planar* array are used to show the focusing effects achievable by tuning its main geometrical and electrical parameters, and the advantages with respect to a conventional NFF *planar* array with the same number of array elements. Some preliminary results have already been presented by some of the authors in [18]–[20].

It is worth mentioning that the phase compensation required to focus the near field radiated by an antenna array can also be obtained by controlling the physical distance between each array element and the assigned focal point, namely using a conformal array. As an example, it is apparent that a constant array phase excitation would suffice for a NFF linear array whose elements are on a circle with its center overlapped to the focal point. In this context, Ohtera [21] showed that a curved slotted waveguide array is effective to get a focusing effect if the phase variation along the guiding structure is properly combined with the waveguide curve shape. More recently, a detailed analysis of a NFF leaky wave array antenna based on a curved slotted substrate integrated waveguide (SIW) has been presented in [22]. In that paper, the authors use the further degree-of-freedom represented by the array linear shape to improve the control of the array focus steering when the latter is achieved through frequency variation. In this context, the multi-panel arrangement of NFF subarrays here proposed may be seen as a *discrete* approximation of a *continuous* curved NFF antenna as those in [21], [22].

This paper is organized as follows. Section II briefly summarizes the radiation characteristics of a planar NFF subarray, which represents the basic element of the multi-panel NFF antenna. Sections III and IV describe the multi-panel arrangement and its focusing characteristics as a function of a set of geometrical and electrical parameters. Subarrays with the focal point along the broadside direction are considered in Sect. III, while in Sect. IV the subarray focal point is allowed to be out of broadside direction. A comparison with a conventional *planar* NFF array is addressed in Section V. Experimental results for a 2-panel NFF array operating at 2.4 GHz are illustrated in Section VI. Conclusions are given in Section VII.

II. FOCUSING CHARACTERISTICS OF A NEAR-FIELD FOCUSED PLANAR SUBARRAY

The building block of the *non-planar* NFF antenna is represented by the NFF *planar* subarray shown in Fig. 1. A survey on the design criteria and performance parameters for planar NFF arrays can be found in [2], [3]. For the reader's convenience, some basic concepts together with the main geometrical and electrical parameters are here concisely summarized. Let us consider a planar subarray made of $N \times M$ identical radiating elements located on the xy-plane of a rectangular

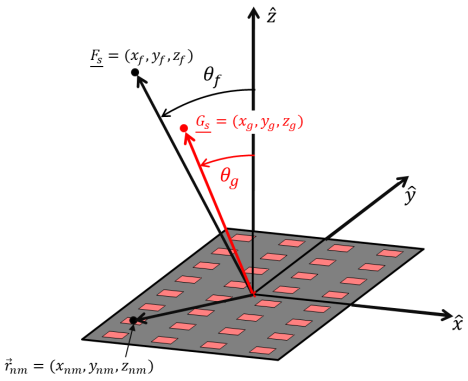

FIGURE 1. The *NXM* NFF subarray placed on the *xy*-plane, with the assigned focal point at $\underline{F_s}$. $\underline{G_s}$ denotes the position of the field peak, and θ_f and θ_g are the angles formed by the broadside direction with $\underline{F_s}$ and $\underline{G_s}$, respectively.

coordinate system (Fig. 1 shows a 4x8 subarray), with a uniform amplitude excitation. To assure in-phase field superposition at the focal point $\underline{F_s} = (x_f, y_f, z_f)$, the following excitation phase ϕ_{nm} must be applied at the nm^{th} radiating element placed at $\vec{r}_{nm}$:

$$\phi_{nm} = k\sqrt{(x_{nm} - x_f)^2 + (y_{nm} - y_f)^2 + z_f^2}, \qquad (1)$$

where k denotes the free-space wavenumber, and $\vec{r}_{nm} = (x_{nm}, y_{nm}, 0)$ is the nm^{th} radiating element position. If the observation point at $\bar{r} = (x, y, z)$ is located outside the reactive near-field region of each radiating element, the net field radiated by the subarray is given by:

$$\bar{E}(\bar{r}) = \sum_{nm} e^{j\phi_{nm}} \frac{e^{-jkR_{nm}}}{R_{nm}} \bar{f}(\theta_{nm}, \phi_{nm}). \qquad (2)$$

In (2), $R_{nm} = k\sqrt{(x - x_{nm})^2 + (y - y_{nm})^2 + z^2}$ is the distance between the observation point and the nm^{th} radiating element, and $\bar{f}(\theta_{nm}, \phi_{nm})$ includes the polarization feature and radiation pattern of the nm^{th} element. In the following, numerical results for the radiated field have been calculated by assuming a cosine-pattern model typically used for a basic linearly-polarized rectangular patch antenna:

$$\bar{f}(\theta, \phi) = \cos\theta \left(\hat{\theta}\cos\phi - \hat{\phi}\sin\phi\cos\theta\right), \text{ with } \theta \leq \frac{\pi}{2} \qquad (3)$$

In the implemented numerical codes, eq. (3) has been included to account for the different spatial position and orientation of each array element with respect to the observation point. It is worth noting that the vector sum in (2) takes into account the polarization mismatching effects, which may not be negligible in the near-field region of large arrays with relatively small focal lengths [2].

In the following numerical results, all the considered subarrays present an interelement separation of $\lambda/2$, with $M = 8$ elements along the y-axis, and $N \leq M$. Then, the maximum antenna size is $D = 8\lambda/2 = 4\lambda$ and the radius of the far-field region can be approximated with $r_{FF} = 2D^2/\lambda = 32\lambda$. As the assigned focal point of each NFF subarray will be placed at a distance $F_s \in [2\lambda, 10\lambda]$, it is always located inside the radiative near-field region of the NFF antenna. It must be pointed out that focal lengths less than 2λ are not considered as the model in (2) loses accuracy in the reactive near-field region of each single radiating element.

Due to the field spreading factor $e^{-jkR_{nm}}/R_{nm}$, the peak of the radiated field does not occur at the focal point where all field contributions sum in phase, but it is located at a point between the antenna aperture and the assigned focal point [2]. For an assigned size of the array, the focal shift (defined as the distance between the actual field peak position and the assigned focal point) vanishes as the focal length reduces. On the contrary, if the focal point approaches the boundary of the array far-field region then the position of the field peak reaches a limit point and the focal shift increases linearly with the focal length [2].

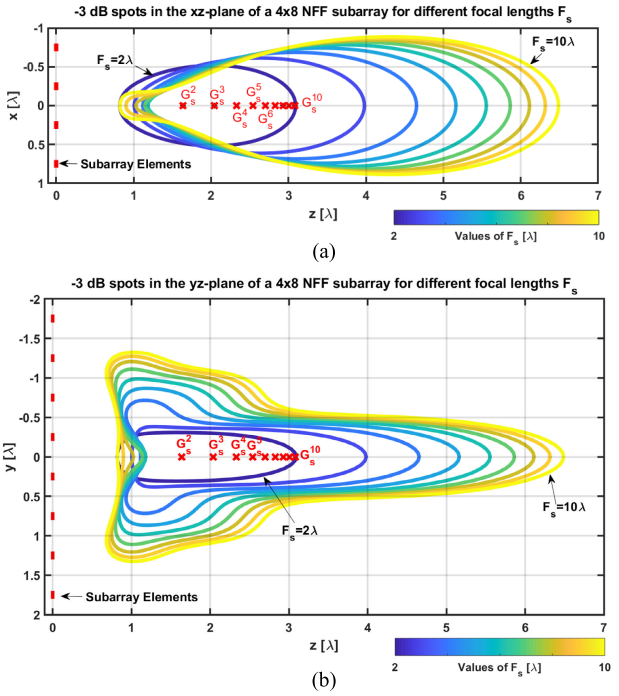

FIGURE 2. Analysis of the -3dB focal spot for a 4×8 planar NFF subarray, for different values of focal point $\underline{F_S}$: (a) xz-plane. (b) yz-plane. The focal length varies in the range $2\lambda \leq F_S \leq 10\lambda$. The red crosses show the field peak position, $G_S^{F_S}$, for each focal length F_S. The red dashed lines along $z = 0$ plane denote the radiating element positions.

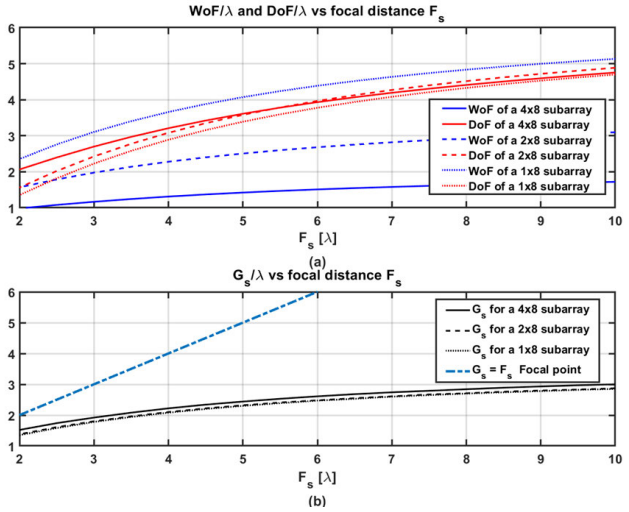

FIGURE 3. (a) WoF/λ, DoF/λ and (b) distance of the field peak from the antenna surface, G_S/λ, vs. the focal length, F_S, for three different subarray dimensions: $N \times M = 1 \times 8$, 2×8 and 4×8. In (b), the blue dashed line corresponds to the equation $G_S = F_S$, and it allows to easily identify the focal shift, which apparently reduces for smaller focal lengths.

As an example, Fig. 2 shows the -3dB contour curves of the focal spot for a 4x8 subarray, in both the xz-plane and yz-plane, for a set of values of the assigned focal length F_s, when the focal point is along the array broadside direction. As expected, the focal spot enlarges as the focal length increases.

To quantify the size of the -3dB focal spot in the xz-plane, Fig. 3a shows WoF and DoF, both normalized to the free-space wavelength, λ, as a function of the normalized

focal length, F_s/λ, for three different planar subarrays: $N \times M = 4 \times 8$, 2×8 and 1×8. Moreover, Fig. 3b shows the distance from the array surface of the field peak, G_s. As expected [2], [3], smaller arrays exhibit larger focal spots, and the distance of the field peak from the assigned focal point (focal shift) is smaller when the term $F_s/\left(2D^2/\lambda\right)$ reduces, namely for shorter focal lengths and larger arrays. Finally, when comparing the focusing performance of the three subarrays, it is apparent that the WoF is the parameter with the largest variations.

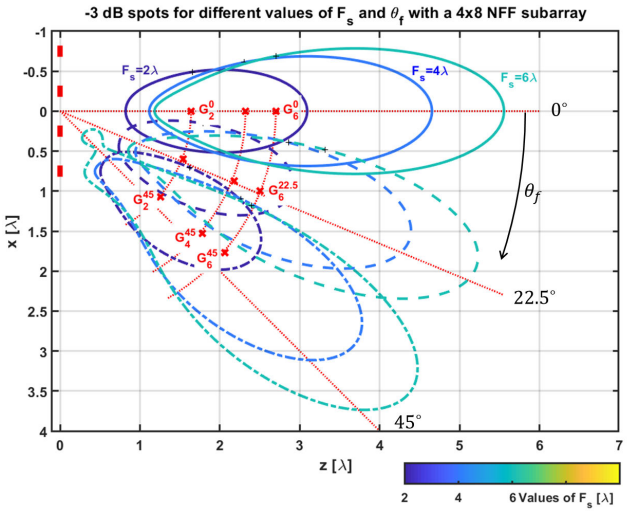

FIGURE 4. **-3dB focal spots in the *xz*-plane for the 4x8 NFF subarray, for different focal lengths F_S ($F_S/\lambda = 2, 4, 6$) and angles θ_f from the array broadside direction ($\theta_f = 0°, 22.5°, 45°$). The red crosses denote the field peak position $G_{F_S}^{\theta_f}$ for each pair (F_S, θ_f).**

Let us now consider more general cases where each subarray may present a focal point along an axis forming an arbitrary angle θ_f with respect to its broadside direction (Fig. 1). In Fig. 4, the -3dB focal spots and the location of the field peak for focal lengths F_s equal to 2λ, 4λ and 6λ, are shown, when the angle θ_f equals to 22.5° and 45°. The results when the subarray focal point is along the broadside direction ($\theta_f = 0°$) are also shown as a reference. For an assigned focal distance F_s, if the angle θ_f increases then the distance G_s does not change significantly meanwhile the angle θ_g is smaller than θ_f. For the case $\theta_f = 45°$, the field peaks appear at an angle $\theta_g \approx 40.5°$. For lower angles θ_f, the separation is smaller; as an example, for $\theta_f = 22.5°$ the location of the field peak is at $\theta_g = 21.9°$. Both DoF and WoF present marginal variations with respect to the results shown in Sect. II and valid for $\theta_f = 0°$.

III. FOCUSING CHARACTERISTICS OF MULTI-PANEL ARRAYS FORMED BY IDENTICAL NFF SUBARRAYS

This section shows the focusing characteristics of a multi-panel array formed by P identical NFF subarrays that are concentrically arranged over a cylindrical boundary of radius a. Each subarray focal point is at a distance F_s from the array surface along its broadside direction ($\theta_f = 0°$).

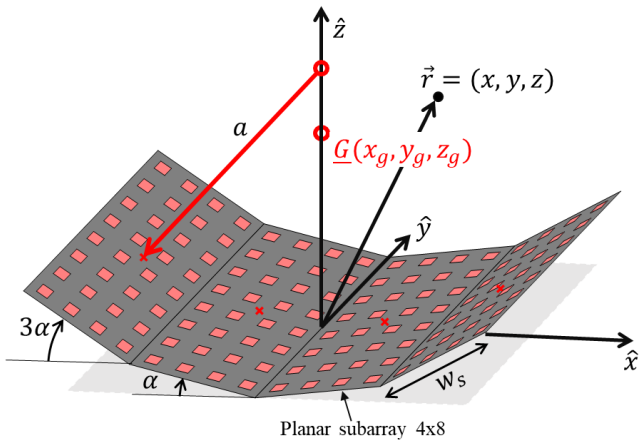

FIGURE 5. **A multi-panel array made of P identical NFF subarrays concentrically arranged over a cylindrical boundary of radius a. For an assigned radius a, the corresponding angle α denotes the rotation of each subarray that determines the final field peak position, $\underline{G}$, and the focal spot shape (DoF and WoF).**

The non-planar array in Fig. 5 is a multi-panel arrangement of P identical NFF planar $N \times M$ subarrays, with adjacent subarrays sharing a common edge along the y-axis, for a total of $P \times N$ 1xM linear subarrays parallel to the y-axis. The P subarrays are arranged symmetrically with respect to the yz-plane, so that the radiated field is symmetric with respect to that plane and the field peak is located along the z-axis. The angle α is directly related with the radius a and the width of each subarray, w_s: $\alpha = \text{asin}\,(2a/w_s)$. Fig. 5 shows an example of a multi-panel antenna configuration where $P = 4$ identical NFF planar subarrays are configured with an α-angle rotation to obtain a narrower focal spot with respect to a planar NFF array with the same number of elements (the same geometry as in Fig. 5 but with $\alpha = 0°$).

Since the identical subarrays are arranged on a cylindrical surface, the focal spot can be perceived as the superposition of the focal spots radiated by the P subarrays, which are simply rotated in the xz-plane. A schematic picture of this field overlapping is represented in Fig. 6, when only three subarrays are considered for clarity. Once both the layout and focal length F_s of the subarrays have been assigned, the distribution of the total field radiated by the multi-panel array can be controlled by changing the radius a. To sum in phase at a given point the contributions from all radiating elements, the radius of the cylindrical surface should be equal to the focal distance of the subarrays, namely $a = F_s$. Nonetheless, to reduce the spot size also accounting for the focal shift effect mentioned in Sect. II, the field peak position of each subarray should be close to the center of the cylindrical surface a $\sim G_s$. Indeed, if $a = G_s$ the total field at the center of the cylindrical surface is given by the in-phase superposition of the subarray contributions, each one corresponding to its local field peak. In Fig. 6, the focal spot for a 3-panel array has been obtained when $F = 5\lambda$ for each subarray, for three different values of the radius a: $a = 4\lambda$, $a = G_s = 2.44\lambda$, $a = 2\lambda$. The results in Fig. 6 demonstrate the effectiveness of the proposed

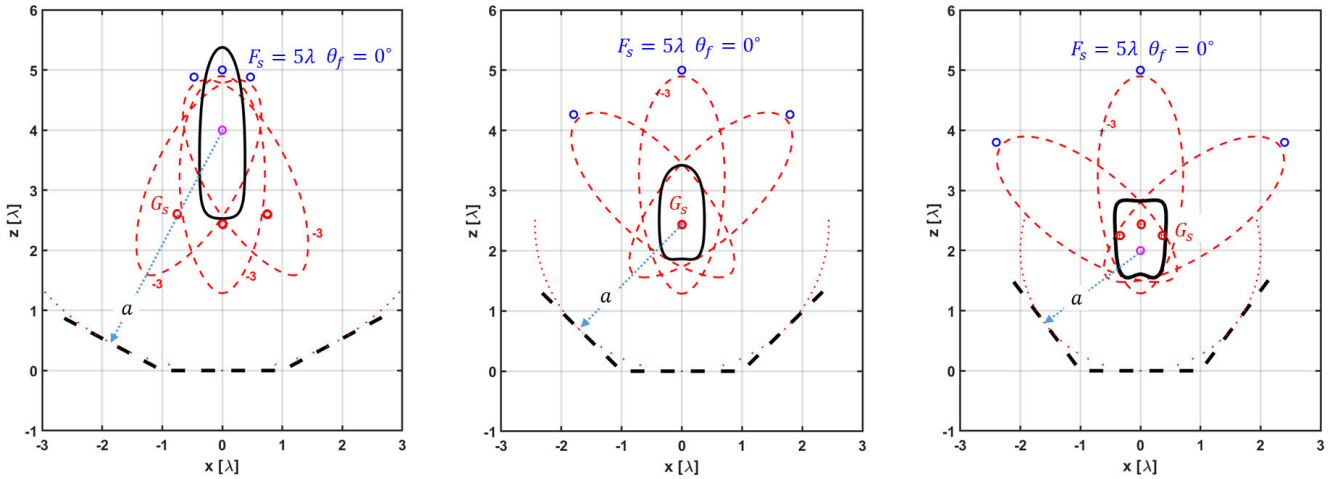

(a) the radius is larger than G_s: $a = 4\lambda$ (b) the radius is equal to G_s: $a = 2.44\lambda$ (c) the radius is smaller than G_s: $a = 2\lambda$

FIGURE 6. **A schematic picture of how the overlapping of the focal spots of three NFF planar subarrays of 4x8 patches (red dashed lines) can be managed to shape the focal spot of the 3-panel NFF array (black continuous line). The three identical subarrays are focused at $F_S = 5\lambda$ in their broadside direction ($\theta_f = 0°$), which corresponds to a position of the field peak at $G_S = 2.44\lambda$. For each subarray, the focal point and the field peak position are denoted by blue and red circles, respectively, while the black sections indicate the position of the patches of the three 4×8 linear subarrays parallel to the y-axis. The focal spot for the whole 3-panel array has been obtained for three different values of the radius a (pink circle denotes the center of the circumference): (a) $a = 4\lambda$; (b) $a = G_S = 2.44\lambda$; (c) $a = 2\lambda$.**

multi-panel arrangement to control the shape of the focal spot. Moreover, it is apparent that the focal spot size gets smaller when the radius a is closer to the field peak distance G_s of NFF subarray ($G_s = 2.44\lambda$) rather than to F_s.

Ideally, the inward radiations of subarray panels that are distributed on the entire cylindrical boundary would result in almost rotationally symmetric focal spots. However, such a full-circle arrangement is often not applicable in real-world scenarios, and then an asymmetric focal spot must be accepted.

In the following, the performance of different multi-panel NFF arrays will be investigated to analyze how the radius of the cylindrical surface influences the size and shape of the -3dB focal spot. The numerical analysis is concentrated on the following parameters: DoF along the z-axis; WoF along the x-axis; position of the field peak amplitude along the z-axis, G; depth-to-width ratio, DWR=DoF/WoF.

As an example, in Fig. 7, the contour curve of the -3dB focal spot of a $P = 2$ panel antenna of 4x8 NFF subarrays is shown, when the focal length of each subarray is $F_s = 10\lambda$, and a varies between 2λ and 10λ. As expected, the size of the focal spot reduces when the radius a is smaller, for subarrays with an assigned focal length F_s. In the same figure, red crosses denote the position of the field peak. It is still apparent that for $a = G_s = 3\lambda$ the focal spot is smaller than for $a = F_s = 10\lambda$.

For a fair comparison, the multi-panel layouts that are considered hereinafter all require 64 radiating elements: $P = 2$ with 4x8-subarrays (2-panel antenna), $P = 4$ with 2x8-subarrays (4-panel antenna), and $P = 8$ with 1x8-subarrays (8-panel antenna). The interelement distance is $d = 0.5\lambda$, along both array axes. It is worth noting that for the two smaller subarrays, $N = 1, 2$, the focusing phase variation

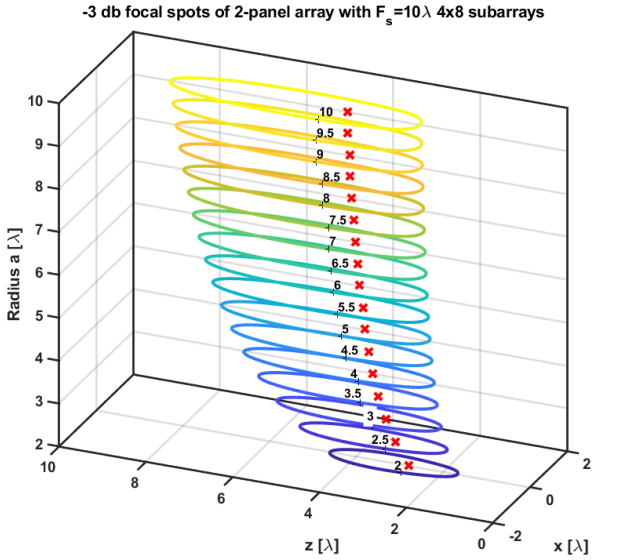

FIGURE 7. **Contour curve of the -3dB focal spot for a 2-panel array. Each 4x8 subarray is characterized by a focal distance $F_S = 10\lambda$ (with a corresponding position of the field peak at $G_S = 3\lambda$). The radius a of the cylindrical surface changes from 2λ to 10λ. The red crosses denote the position of the field peak inside the focal spot, at a distance G from the array vertex.**

occurs along the y-axis only, so requiring a simpler feeding network design with respect to the 4x8 subarray ($N = 4$). For each multi-panel NFF antenna, contour plots of DoF, WoF and DWR are shown in Figs. 8 and 9, as a function of both the subarray focal length, F_s, and the radius a. In each plot, two additional curves are added to indicate the focusing performance that can be achieved when using the two following design criteria for the radius a: $a = F_s$ and $a = G_s$.

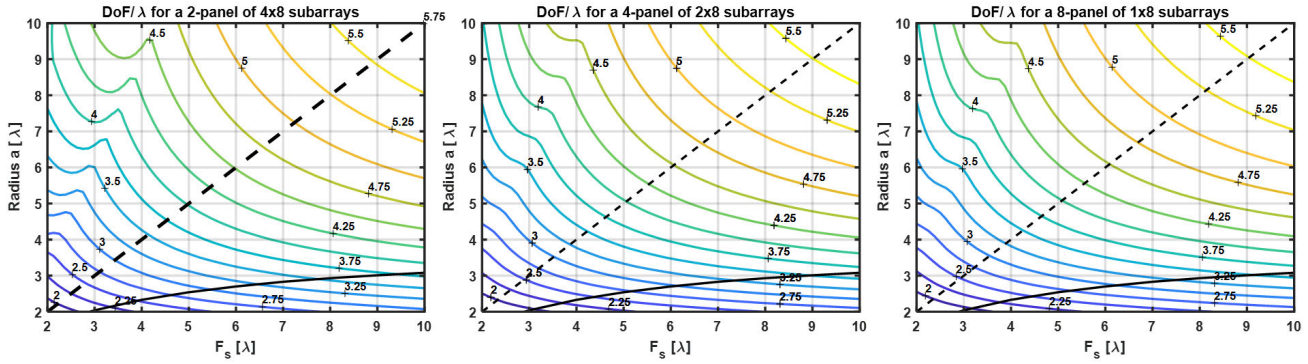

FIGURE 8. Contour plot of the depth of focus (DoF) in the *xz*-plane vs. the focal length of the subarray and the radius *a*, for three multi-panel arrangements. Additional curves are added to indicate the focusing performance that can be achieved when using the two following design criteria for the radius *a*: $a = F_S$ (black dashed line) and $a = G_S$ (black continuous line).

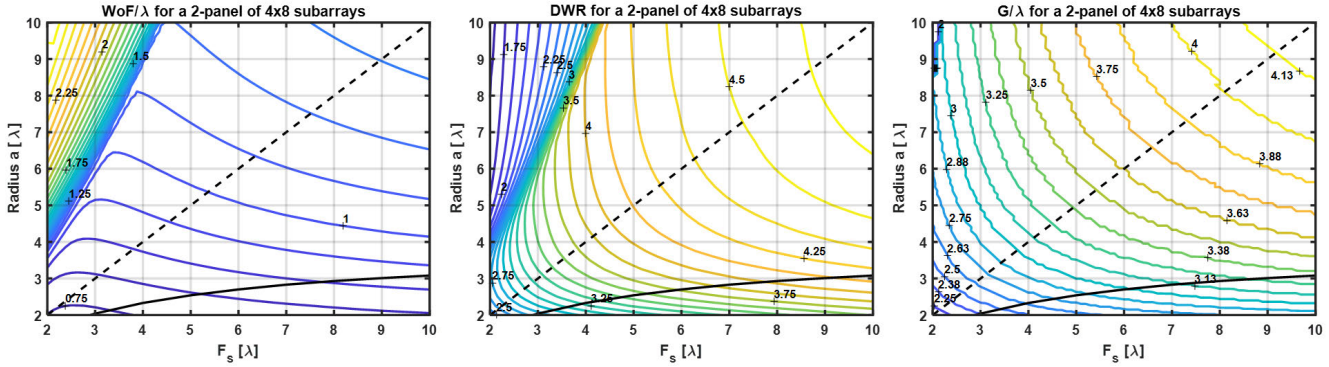

FIGURE 9. (a) Contour plots for the width of focus (WoF) along the *x*-axis, (b) DWR=DoF/WoF and (c) distance of the field peak from the antenna vertex *G*. All the results are represented vs. the focal length of the subarray and the radius *a*, for the 2-panel antenna configuration. Additional curves are added to indicate the focusing performance that can be achieved when using the following design criteria for the radius *a*: $a = F_S$ (black dashed line); $a = G_S$ (black continuous line).

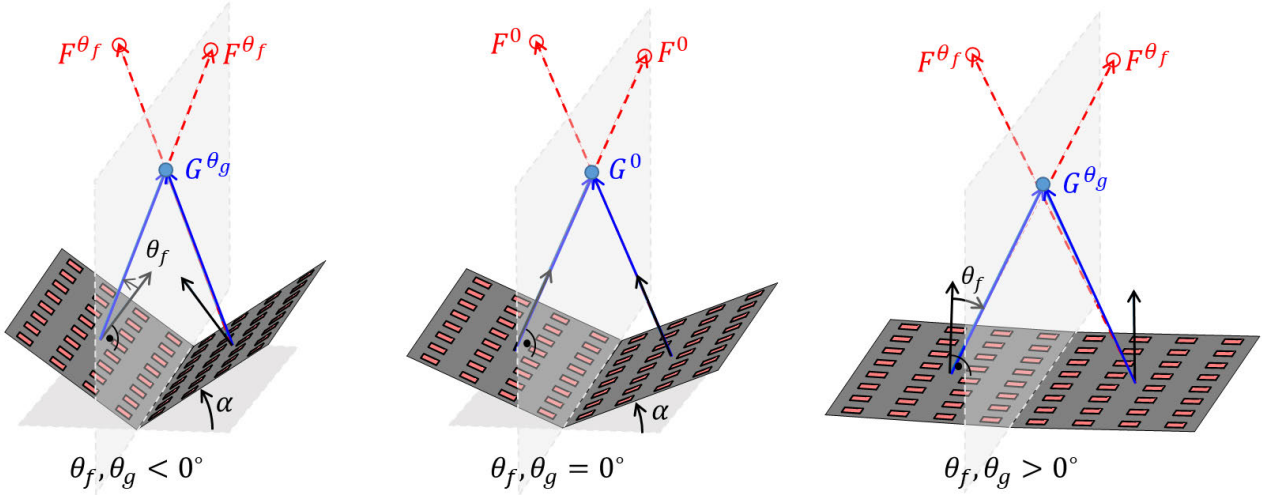

FIGURE 10. Different configurations for multi-panel arrays formed with subarrays exhibiting a focal point at an angle θ_f respect to their broadside direction. (a) Subarray with a focal point at F^{θ_f} forming angle θ_f in the CCW direction respect to the broadside direction (θ_f will be considered negative in this configuration). (b)) Subarray with a focal point at F^{θ_f} in the broadside direction ($\theta_f = 0°$, as considered in Sect III). (c) Subarray with a focal point at F^{θ_f} forming angle θ_f in the CW direction respect to the broadside direction. (θ_f will be considered positive in this configuration).

It appears that the choice of $a = G_s$ guarantees more compact focal spots. From Fig. 8, it is worth noting that the curves for the DoF look similar when changing the number of array panels. Same consideration applies to the curves for WoF, DWR and *G*. Due to the lack of space, only the results for the 2-panel antenna with 4x8 subarrays are shown in Fig. 9.

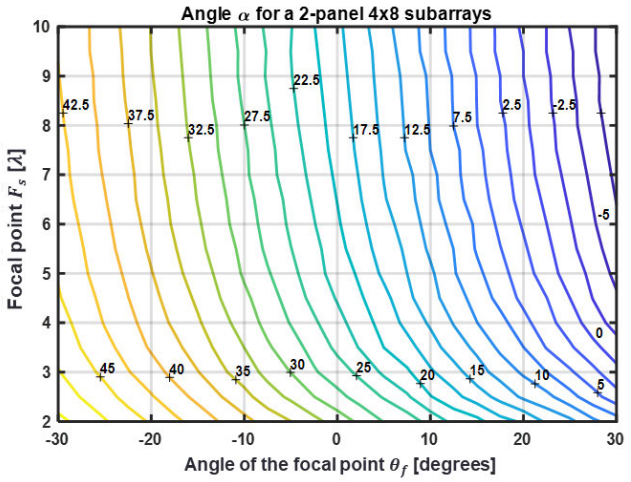

FIGURE 11. Values of angle α to set-up the 2-panel array of 4×8 subarrays with subarray field peak overlapping along the z-axis, as a function of the focal length F_s and the θ_f angle.

The cylindrical arrangement with small values of the radius a is effective to reduce the focal spot size; indeed, DoF and WoF can be as small as 3λ and λ, respectively. As far as the DWR is concerned, from results in Fig. 9(b) it appears that is impossible to achieve values down to 1, namely an almost symmetric focal spot in the xz-plane. Values of DWR less than 2 can be obtained with large values of the radius a but those imply larger focal spots.

Fig. 9(c) shows the distance from the antenna vertex of the field peak position, G. Let us consider the values of G that are obtained when the design criteria $a = G_s$ is adopted; in this case, the field peak of the whole multi-panel antenna is expected to coincide with the local field peak of the each subarray $G = \sqrt{a^2 + (w_s/2)^2} = \sqrt{G_s^2 + (w_s/2)^2}$, where w_s denotes the subarray width (Fig. 5). Above condition is verified by the numerical results in Fig. 9c.

Based on the results for the considered multi-panel configurations, it can be concluded that the NFF multi-panel antenna performance mainly depends on the radius a and subarray focal distance F_s, rather on the number of subarrays. Moreover, the NFF antenna with just two panels may be an acceptable tradeoff between the focusing performance and the mechanical complexity of the proposed multi-panel antenna. On the other hand, it should be considered that, for an assigned total number of linear arrays along the y-axis, using only two panels implies larger NFF subarrays and then a more complex phase-shifting feeding network for each subarray.

IV. NFF SUBARRAYS WITH FOCAL POINT AT A θ_F ANGLE FROM THE BROADSIDE DIRECTION

In this section, NFF subarrays with a focal point at a direction forming an angle $\theta_f \neq 0$ with the subarray broadside direction (as shown in Fig. 4) will be analyzed. The study will be limited to 2-panel arrays (namely, $P = 2$ 4×8 subarrays) with the field peaks from subarrays overlapping at the same point along the z-axis. It is apparent that, in general, this geometrical configuration does not allow to use identical subarrays; however, since the two subarrays are apparently required to have a specular radiation with respect to the yz-plane (see Fig. 10), the feeding network implementation of the two subarrays does not change. The different geometries being here analyzed are shown in Fig. 10, where the angle α is always chosen to guarantee overlapping of the subarray field peaks:

- Fig. 10(a): two symmetric subarrays with their focal point at $\theta_f < 0°$; the angle α is greater with respect to the set-up in Fig. 10(b);
- Fig. 10(b): two identical subarrays with the focal point at their broadside position, $\theta_f = 0°$ (as those in Sect. III);
- Fig. 10(c): two symmetric subarrays with their focal point at $\theta_f > 0°$; a smaller angle α ($\alpha \approx 0°$) is needed with respect to the set-up in Fig. 10(b).

When compared to the planar NFF array, these 2-panel configurations give the possibility of achieving smaller focal spots and field peaks closer to the antenna surface. To study the behavior of above multi-panel configurations, a 2-panel

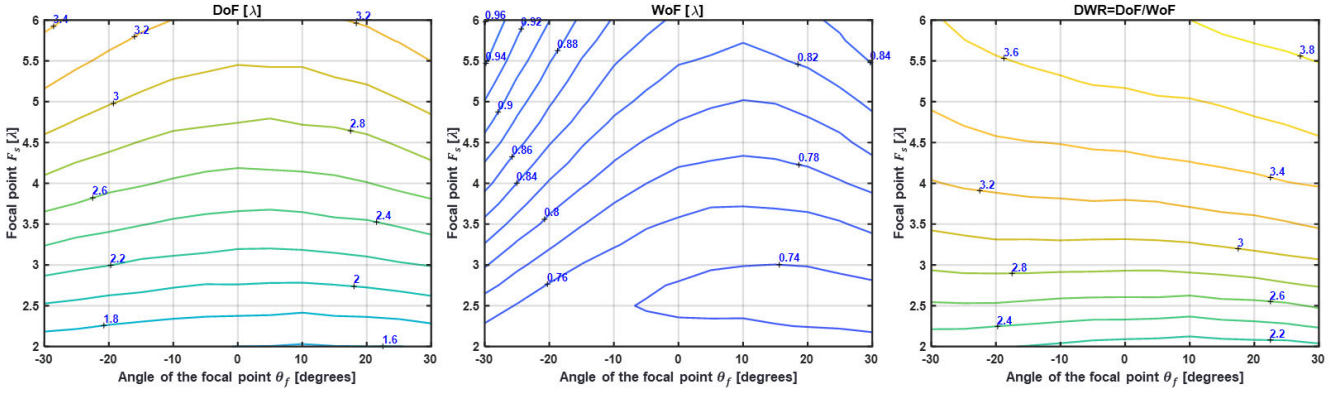

FIGURE 12. (a) Contour plot of the depth of focus (DoF), (b) the width of focus (WoF) and (c) the DWR=DoF/WoF. The variation of the three parameters is shown as a function of the focal point distance F_s and its angle θ_f respect to the broadside direction of each NFF subarray.

antenna made of two 4x8 subarrays has been considered, with focal length F_s ranging from 2λ up to 6λ, and $\theta_f \in [-30°, 30°]$. Fig. 11 shows the value of α needed to get a 2-panel configuration with the subarray field peaks overlapped along the z-axis, as shown in Fig. 10. As the value of θ_f increases (namely, from the configuration shown in Fig. 10(a) to the one shown in Fig. 10(c)), the required angleα decreases, eventually reaching a near-flat configuration. As the focal length F_s increases, while maintaining fixed the angle θ_f, the required values for α are smaller, due to the fact that the field peak position moves away from the subarray surface (Fig. 10).

Fig. 12 presents the variation of DoF, WoF and DWR, showing that lower values of DoF and WoF can be obtained when considering values of θ_f closer to the broadside direction ($\theta_f = 0$), meanwhile the ratio DWR does not present significant variations, mainly for focal distances F_s between 2λ and 4λ.

When the multi-panel array field-peak position and amplitude level are analyzed for all above configurations, it can be observed that, for a given value of the focal distance F_s, the field peak position gets closer to the antenna as the value of θ_f increases (results in Fig. 13 (a)). Regarding to the field peak position (Fig. 13(b)), for a given value of focal distance F_s, the maximum field level is obtained when the subarrays are configured with their focal point close to their broadside direction. As an example, for a 2-panel formed by 4×8 subarrays designed with a focal point at 2λ with $\theta_f = 30°^X$, and setting $\alpha = 8.5°$ (Fig. 13), the multi-panel array exhibits the following features: DoF≈ 1.65λ, WoF≈ 0.75λ and a DWR≈ 2.2λ (Fig. 14). This configuration will produce a field peak located at 1.6λ from the edge of the array in the broadside direction (Fig. 13(a)).

From above results, it can be concluded that the multi-panel configuration with subarrays with their focal point close to their broadside direction leads to higher field peak level and smaller DoF and WoF. Other configurations using subarray with focal points located at angles apart from the broadside direction ($\theta_f \neq 0$) can be used to get the field peak position closer to the antenna edge, also allowing more flattened configurations than the ones shown in Sect. III.

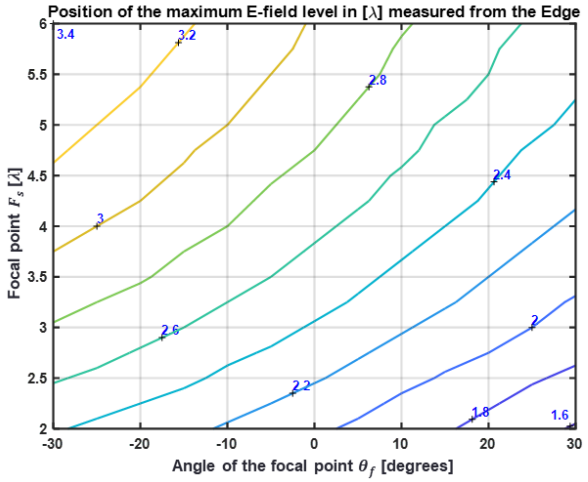

(a)

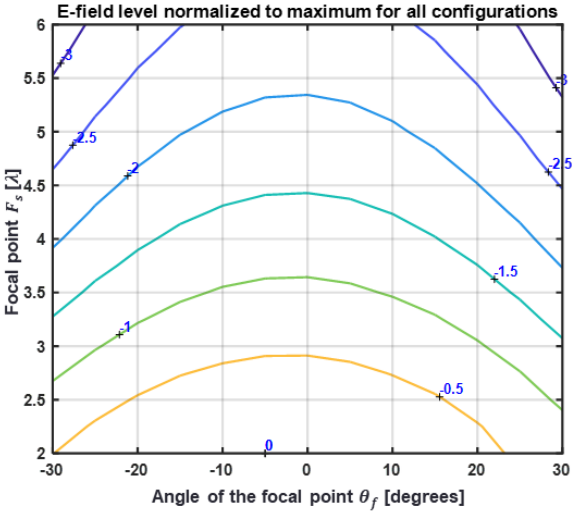

(b)

FIGURE 13. (a) Contour plot of the distance of the field peak from the edge of the multi-panel array, (b) the normalized E-field peak level of the multi-panel array. Both parameters are shown as function of the focal point distance F_s and its angle θ_f respect to the broadside direction, of each NFF subarray.

V. MULTI-PANEL ARRAY VS. PLANAR ARRAY

The focusing performance achieved by the multi-panel array is here compared versus that one of a conventional planar NFF array. For a fair comparison, we have considered an 8x8 NFF planar array, so that all the compared NFF antennas are made by 64 radiating elements and have the same size along the y-axis. Also, the 8x8 NFF planar array is characterized by the same interelement distance ($d = \lambda/2$) as for the subarrays in previous sections.

It is worth noting that, with respect to the 8x8 planar array, the multi-panel NFF arrays have a smaller aperture in the xy-plane (the latter depending on the angle α), and a simpler phase-shifting feeding network as the P panels are identical or symmetrical considering configurations of the previous Sect. III or Sect. IV, respectively. On the other hand, above advantages are balanced by the more complex mechanical realization of the multi-panel antenna. In other words, the degree-of-freedom represented by a larger number of phase excitations to be controlled is here exchanged with the control of the focal spot allowed by the angle α of the cylindrical arrangement.

In Fig. 14(a), the DoF, WoF, DWR and the position of the field peak, G, are shown as a function of the focal length F_s, for the NFF 8x8 planar array. When comparing these results with those obtained with two different configurations of a 2-panel NNF array, it can be concluded that:

- the multi-panel arrangement is effective to reduce the DoF;

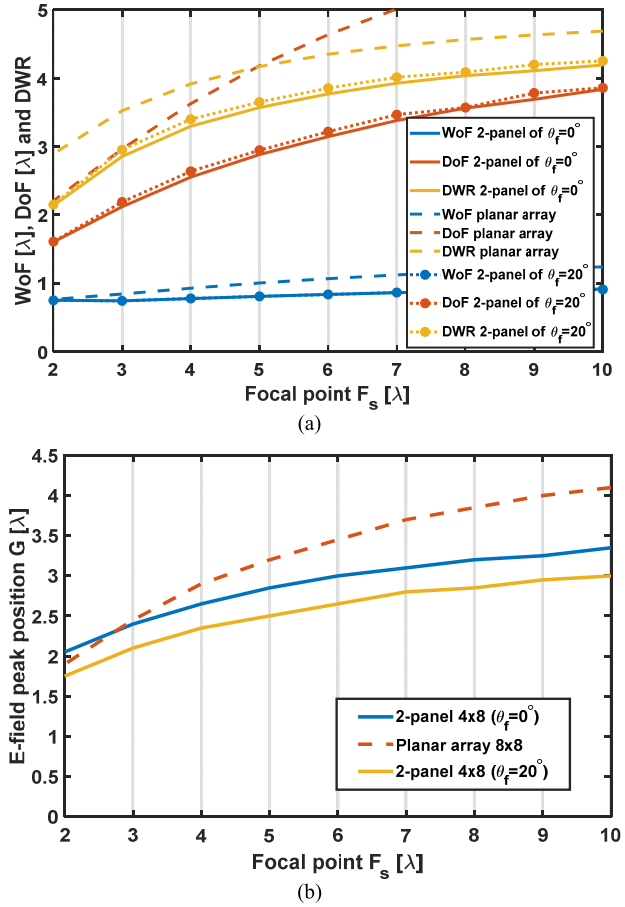

FIGURE 14. **(a) DoF and WoF in the *xz*-plane, DWR and (b) distance of the field peak position from the antenna vertex, *G*, vs. the focal length, for an 8x8 NFF planar array and two different configurations of a 2-panel array: $\theta_f = 0°$ and $\theta_f = 20°$.**

- the WoF is around λ, for both the multi-panel antennas and 8x8 planar array;

- a proper combination of the radius a and focal length F_s can be used to get DWR values less than those achievable with the planar array, for which DWR>3. Another advantage of the multi-panel NFF antennas is that it allows to obtain a field peak position closer to the antenna surface compared to the conventional NFF planar array (Fig. 14(b)).

VI. VALIDATION THROUGH FULL WAVE SIMULATIONS AND EXPERIMENTAL MEASUREMENTS

Two planar 4×8 subarrays, where the radiating elements are linearly polarized patches operating at the 2.4 GHz ISM band, are arranged to realize a 2-panel NFF antenna. The single radiating element is a coaxial-fed patch realized on FR4 substrate (1.6mm thick, $\epsilon_r = 4.4$). The interelement distance is equal to $d = \lambda/2 = 6.25$ cm. Considering the results of previous sections, two identical 4x8 subarray has been realized with a feeding network implementing a focal distance $F_s = 8\lambda = 100$ cm at the broadside direction ($\theta_f = 0°$). For an angle $\alpha = 17.4°$ (corresponding to a radius $a \approx 3.2\lambda = 40$ cm) the field peak is at 41.9 cm from the antenna vertex.

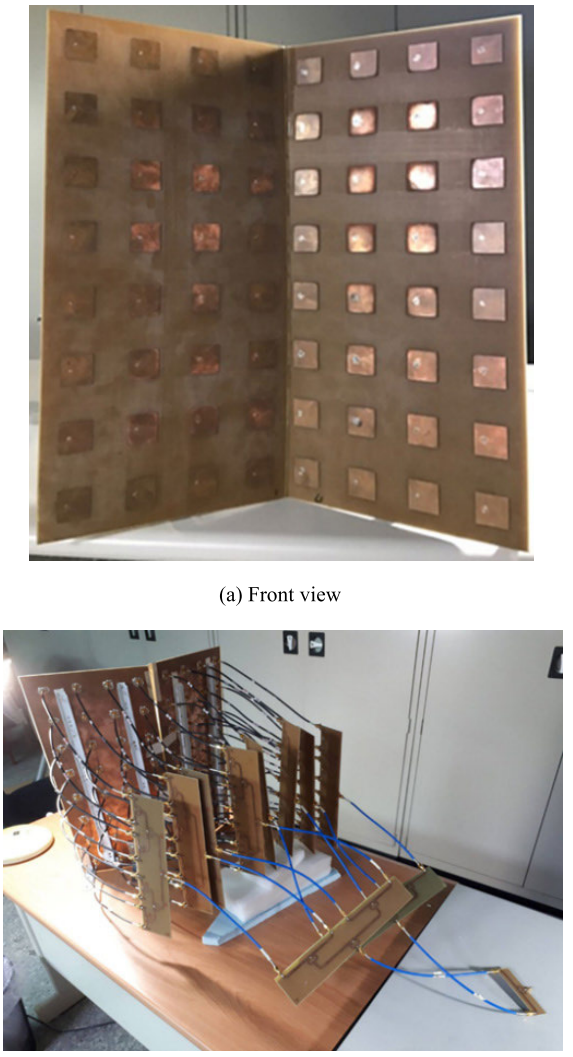

(a) Front view

(b) Rear view of the antenna prototype

FIGURE 15. **Photos of the 2.4GHz 2-panel NFF array in the Microwave Laboratory of the National Taiwan University. (a) Front view showing the two panels, each one with 4x8 linearly polarized coaxial-fed patches. (b) Rear view showing the array feeding network.**

Near-field measurements have been performed by an NSI near-field planar scan system using a WR430 waveguide probe, at the measurement facilities of the Yuan Ze University, Taiwan. Photos of the prototypes are shown in Fig. 15. The phase-shifting feeding network is realized by using coaxial cables with 3dB Wilkinson power dividers. The required phase shifts are implemented by using coaxial cables of different length. Fig. 16(a)∼(c) show the normalized contour patterns on the *yz*-plane, *xz*-plane and plane at $z = 41.9$ cm from the antenna vertex.

As for the patterns on the *yz*-plane and *xz*-plane, measurements agree quite well with the simulations. Measured DoF and WoF are found to be equal to 49 cm and 15 cm, respectively, with DWR=3.3, which all are in good agreement with the simulated results. Indeed, from the analytical solution presented in Sect.III it comes up that DoF=44 cm

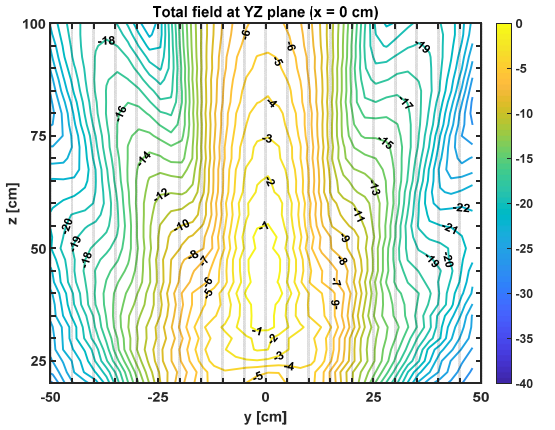

(a) yz plane

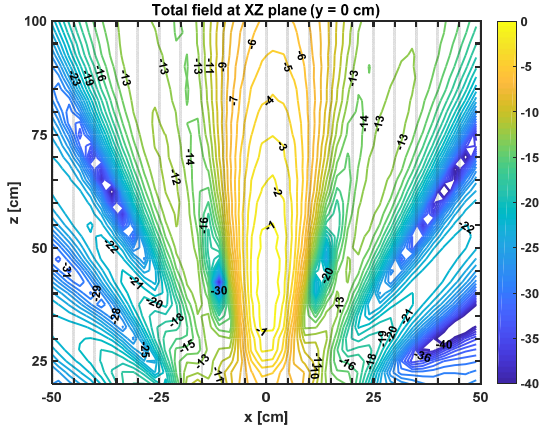

(b) xz-plane

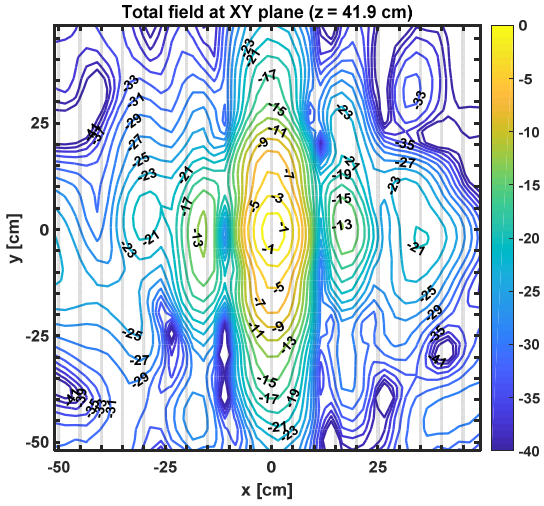

(c) plane at z=41.9 cm

FIGURE 16. **Measured near field normalized contoured patterns for the prototype of the 2-panel array: (a) *yz*-plane; (b) *xz*-plane; (c) $z = 42$ cm. The contours are plotted in a 1dB step in (a) and (b), and are in a 2 dB step in (c).**

and WoF=13.6 cm, meanwhile full-wave numerical simulations performed with Ansoft HFSS (High Frequency Electromagnetic Field Simulation) give DoF=44 cm and WoF=12.5 cm. DWR is close to 3.52 for numerical results.

VII. CONCLUSION

Near-field focused arrays in a multi-panel configuration have been investigated, with the main goal of showing their effectiveness to shape the -3dB focal spot. The first proposed NNF antenna consists of P identical NFF planar subarrays that are arranged on a cylindrical surface, where each subarray exhibits its focal point at broadside direction. It has been shown that the radius of the cylindrical surface and the focal length of the subarrays can be chosen to get a more symmetrical focal spot, with respect to conventional planar NFF arrays. Using identical panels allows to reduce the complexity of the feeding network with respect to a NFF planar array with the same total number of array elements, where each radiating elements could be properly phased to get an in-phase superposition at the assigned focal point. The loss in terms of degrees-of-freedom available for controlling the focal spot shape (array feeding currents) is overcompensated by the cylindrical structure, at the expenses of a slightly more complex antenna mechanical layout.

The second proposed NFF antenna consists of two symmetric panels with their corresponding focal points out of the broadside direction. The panels are set up with a geometrical configuration to overlap their field peaks. Respect to the configuration with identical subarrays, this one allows having flatter configurations while keeping similar values of DoF and WoF. This layout also permits to move the field peak position closer to the antenna surface.

To limit the computational time while accounting for a relatively wide range of potential configurations, the systematic numerical analysis has been performed by a simple array analytical model, where the contribution of each array element includes only the term $1/r$ and a cosine-like pattern, and array mutual coupling is neglected. On the other hand, its effectiveness has been verified through a set of full-wave numerical simulations and measurements on a 2.4GHz 2-panel array prototype.

Due to space limitations, the effects on the focal spot size and shape of further geometrical parameters (such as the interelement distance or the array length along the cylinder axis) have not been included in this paper, but they can be inferred by accounting for the results for conventional planar NFF arrays [2], [3].

In a future work, the proposed layout will be combined with advanced synthesis techniques developed for NFF planar arrays. Finally, the effectiveness of the multi-panel arrangement here proposed will be tested in the context of multi-focus [23] and reconfigurable [24] near-field focused arrays.

REFERENCES

[1] P. Nepa, A. Buffi, A. Michel, and G. Manara, "Technologies for near-field focused microwave antennas," *Int. J. Antennas Propag.*, vol. 2017, Mar. 2017, Art. no. 7694281.

[2] P. Nepa and A. Buffi, "Near-field-focused microwave antennas: Near-field shaping and implementation." *IEEE Antennas Propag. Mag.*, vol. 59, no. 3, pp. 42–53, Jun. 2017.

[3] A. Buffi, P. Nepa, and G. Manara, "Design criteria for near-field-focused planar arrays," *IEEE Antennas Propag. Mag.*, vol. 54, no. 1, pp. 40–50, Feb. 2012.

[4] D. Blanco, J. L. Gómez-Tornero, E. Rajo-Iglesias, and N. Llombart, "Radially polarized annular-slot leaky-wave antenna for three-dimensional near-field microwave focusing," *IEEE Antennas Wireless Propag. Lett.*, vol. 13, pp. 583–586, 2014.
[5] A. J. Martinez-Ros, J. L. Gómez-Tornero, F. J. Clemente-Fernández, and J. Monzó-Cabrera, "Microwave near-field focusing properties of width-tapered microstrip leaky-wave antenna," *IEEE Trans. Antennas Propag.*, vol. 61, no. 6, pp. 2981–2990, Jun. 2013.
[6] A. J. Martinez-Ros, J. L. Gómez-Tornero, V. Losada, F. Mesa, and F. Medina, "Non-uniform sinusoidally modulated half-mode leaky-wave lines for near-field focusing pattern synthesis," *IEEE Trans. Antennas Propag.*, vol. 63, no. 3, pp. 1022–1031, Mar. 2015.
[7] R. G. Ayestarán, "Fast near-field multifocusing of antenna arrays including element coupling using neural networks," *IEEE Antennas Wireless Propag. Lett.*, vol. 17, no. 7, pp. 1233–1237, Jul. 2018.
[8] G. G. Bellizzi, D. A. M. Iero, L. Crocco, and T. Isernia, "Three-dimensional field intensity shaping: The scalar case," *IEEE Antennas Wireless Propag. Lett.*, vol. 17, no. 3, pp. 360–363, Mar. 2018.
[9] D. A. M. Iero, L. Crocco, and T. Isernia, "Constrained power focusing of vector fields: An innovative globally optimal strategy," *J. Electromagn. Waves Appl.*, vol. 29, pp. 1708–1719, Jul. 2015.
[10] G. G. Bellizzi, M. T. Bevacqua, L. Crocco, and T. Isernia, "3-D field intensity shaping via optimized multi-target time reversal," *IEEE Trans. Antennas Propag.*, vol. 66, no. 8, pp. 4380–4385, Aug. 2018.
[11] H.-T. Chou and Z.-C. Tsai, "Near-field focus radiation of multibeam phased array of antennas realized by using modified rotman lens beamformer," *IEEE Trans. Antennas Propag.*, vol. 66, no. 12, pp. 6618–6628, Dec. 2018.
[12] I. Iliopoulos, B. Fuchs, R. Sauleau, P. Pouliguen, P. Potier, and M. Ettorre, "On the use of convex optimization for electromagnetic near-field shaping," in *Proc. Eur. Conf. Antennas Propag. (EUCAP)*, 2017, pp. 1013–1016.
[13] I. Iliopoulos, B. Fuchs, R. Sauleau, P. Pouliguen, P. Potier, and M. Ettorre, "Scalar near-field focusing in lossy media," in *Proc. Int. Conf. Electromagn. Adv. Appl. (ICEAA)*, Verona, Italy, 2017, pp. 718–721.
[14] W. Wang, H. Gao, Y. Wu, and Y. Liu, "Impact of amplitude weights on power focusing for near-field-focused planar arrays," *Int. J. RF Microw. Comput.-Aided Eng.*, vol. 28, Aug. 2018, Art. no. e21268.
[15] I. Iliopoulos, M. Casaletti, R. Sauleau, P. Pouliguen, P. Potier, and M. Ettorre, "3-D shaping of a focused aperture in the near field," *IEEE Trans. Antennas Propag.*, vol. 64, no. 12, pp. 5262–5271, Dec. 2016.
[16] R. Cicchetti, A. Faraone, and O. Testa, "Energy-based representation of multiport circuits and antennas suitable for near- and far-field syntheses," *IEEE Trans. Antennas Propag.*, vol. 67, no. 1, pp. 85–98, Jan. 2019.
[17] R. Cicchetti, A. Faraone, and O. Testa, "Near field synthesis based on multi-port antenna radiation matrix eigenfields," *IEEE Access*, vol. 7, pp. 62184–62197, 2019.
[18] H.-T. Chou, J.-W. Liu, C.-Y. Liu, and P. Nepa, "Focusing characteristics of near-field radiations from multi-panels of phased array of antennas in circularly cylindrical arrangement," in *Proc. Int. Symp. Antennas Propag. (ISAP)*, Phuket, Thailand, 2017, pp. 1–2.
[19] H.-T. Chou and P. Nepa, "Multi-facet focused microwave antennas," in *Proc. IEEE-APS Top. Conf. Antennas Propag. Wireless Commun. (APWC)*, Cairns, QLD, Australia, Sep. 2016, pp. 294–297.
[20] H.-T. Chou and P. Nepa, "Near-field focused radiation by two edge-coupled microstrip antenna arrays," in *Proc. URSI Int. Symp. Electromagn. Theory (EMTS)*, Aug. 2016, pp. 709–712.
[21] I. Ohtera, "Focusing properties of a microwave radiator utilizing a slotted rectangular waveguide," *IEEE Trans. Antennas Propag.*, vol. 38, no. 1, pp. 121–124, Jan. 1990.
[22] Y. F. Wu and Y. J. Cheng, "Proactive conformal antenna array for near-field beam focusing and steering based on curved substrate integrated waveguide," *IEEE Trans. Antennas Propag.*, vol. 67, no. 4, pp. 2354–2363, Apr. 2019.
[23] J. Alvarez, R. G. Ayestaran, G. Leon, L. F. Herran, A. Arboleya, J. A. Lopez-Fernandez, and F. Las-Heras, "Near field multifocusing on antenna arrays via non-convex optimisation," *IET Microw. Antennas Propag.*, vol. 8, no. 10, pp. 754–764, Jul. 2014.
[24] O. Yurduseven, D. L. Marks, J. N. Gollub, D. R. Smith, "Design and analysis of a reconfigurable holographic metasurface aperture for dynamic focusing in the Fresnel zone," *IEEE Access*, vol. 5, pp. 15055–15065, 2017.

HSI-TSENG CHOU (F'12) received the B.S. degree from National Taiwan University, Taiwan, in 1988, and the M.S. and Ph.D. degrees from The Ohio State University (OSU), in 1993 and 1996, respectively, all in electrical engineering.

He was a Graduate Research Associate and a Postdoctoral Researcher with the ElectroScience Laboratory (ESL), OSU, from 1991 to 1996 and from 1996 to 1998, respectively. He is currently appointed as a Distinguished Professor with the Graduate Institute of Communication Engineering and the Department of Electrical Engineering, National Taiwan University. He has published more than 493 journals and conference articles. He holds 40 patents. His research interests include wireless communication networks, antenna design, antenna measurement, electromagnetic scattering, and asymptotic high frequency techniques, such as uniform geometrical theory of diffraction (UTD), novel Gaussian beam techniques, and UTD-type solution for periodic structures.

Dr. Chou is a Fellow of the IET and an Elected Member of the URSI International Radio Science US Commission B. He received many awards to recognize his distinguished contributions in the technological developments. He was elected as one of the nation's ten outstanding young persons by the Junior Chamber International, in 2004, the National Young Person Medal from the China Youth Corps of Taiwan, in 2005, and as one of the top ten rising stars in Taiwan by Central News Agency of Taiwan. Some important ones includes the Distinguished Contribution Award in promoting inter-academic and industrial cooperation from the Ministry of Education, the Distinguished Engineering Professor Award from the Chinese Institute of Engineers, the Distinguished Electrical Engineering Professor Award from the Chinese Institute of Electrical Engineering, the University's Industrial Economics Contribution Award, in 2008, the National Industrial Innovation Awards-Key Technology Elite Award, in 2011, and the Industrial-Academia Collaboration Award, in 2017, from Ministry of Economics. He received the Best Chapter Award, in 2012, and the IEEE Technical Field Undergraduate Teaching Award, in 2014. He also received the Outstanding Branch Counselor Awards from the IEEE, including the IEEE headquarter, R-10, and Taipei Section. He has served as the Chair for the IEEE AP-S Taipei Chapter. He is also the Chair of the EMC-S Taipei Chapter.

MARCOS R. PINO was born in Vigo, Spain, in 1972. He received the M.Sc. and Ph.D. degrees in telecommunication engineering from the University of Vigo, Vigo, in 1997 and 2000, respectively. In 1998, he was a Visiting Scholar with the ElectroScience Laboratory, The Ohio State University, Columbus, OH, USA. From 2000 to 2001, he was an Assistant Professor with the University of Vigo. Since 2001, he has been with the Electrical Engineering Department, University of Oviedo at Gijón, Gijón, Spain, where he is currently an Associate Professor, teaching courses on communication systems and antenna design. His current research interests include antenna design, measurement techniques, and efficient computational techniques applied to EM problems, such as evaluation of radar cross section or scattering from rough surfaces.

PAOLO NEPA received the Laurea (Ph.D.) degree *(summa cum laude)* in electronics engineering from the University of Pisa, Italy, in 1990.

In 1998, he was a Visiting Scholar with the ElectroScience Laboratory (ESL), The Ohio State University (OSU), Columbus, OH, USA, supported by a grant of the Italian National Research Council (CNR), where he was involved in the research on efficient hybrid techniques for the analysis of large antenna arrays. Since 1990, he has been with the Department of Information Engineering, University of Pisa, where he is currently a Full Professor. He also coauthored almost 100 international journal articles and more than 200 international conference contributions. He also coauthored three chapters in international books and one European patent. His main research interests include the design of wideband and multiband antennas, mainly for base stations and mobile terminals of communication systems and in the design of antennas optimized for near-field coupling and focusing. He is also involved in channel characterization, wearable antenna design, and diversity scheme implementation for body-centric communication systems. In the context of UHF-RFID systems, he is working on techniques and algorithms for radiolocalization of either tagged objects or readers.

Dr. Nepa has been a member of the Local Organizing Committee of the 2004 URSI EMTS, Pisa, Italy. He is also a member of the Technical Advisory Board of URSI Commission B-Fields and Waves and the Italian Society of Electromagnetism (SIEM). He received the Young Scientist Award from the International Union of Radio Science, Commission B, in 1998. He is also the General Chair of the IEEE RFID-TA 2019 International Conference. Since October 2016, he has been serving as an Associate Editor for the IEEE Antennas and Wireless Propagation Letters.

CHANG-YI LIU was born in Taipei, Taiwan, in 1992. He received the B.S. degree in electrical engineering from the Department of Electrical Engineering, Feng Chia University, Taichung, Taiwan, in 2015, and the M.S. degree from the Department of Communication Engineering, Yuan Ze University, Taoyuan, Taiwan, in 2017. He is currently with Yuan Ze University, and is also a Senior Research and Development Engineer with Wistron Company, Taiwan. His research interests include near-field focus (NFF) antennas for RFID applications and antenna design for mobile communications.